Simulation of the Beam–Plasma Instability in a Finite-Length System

A. T. Lin and J. E. Rowe

Department of Electrical and Computer Engineering, The University of Michigan, Ann Arbor, Michigan 48104

(Received 16 August 1971; final manuscript received 14 February 1972)

The electron and ion beam–plasma instabilities in a one-dimensional finite-length system are studied by computer simulation methods using the discrete charge-sheet model. The results obtained using a one-component model indicate that the region of highly concentrated oscillation energy (due to a beam–plasma instability) near the beam entrance plane shrinks with time to a limiting value and then expands to form a stationary electric-field distribution. The frequency spectrum analysis of the electric field shows that only the first few harmonics of electron plasma oscillations have been excited and only these harmonics have amplitudes significantly above the noise level in the nonlinear region. In the experiment on the ion-beam interaction with a plasma, the plasma electrons and ions achieve greater heating in comparison with the heating resulting from the interaction between an electron beam and a plasma, because the heavier ion mass yields a larger energy source, a low rate of decrease of the mean ion-beam speed, and reduced thermal spreading of the beam particles. The excited electron plasma oscillations are found to dissipate into ion-density fluctuations whenever the amplitude exceeds some threshold value.

I. INTRODUCTION

Most of the existing numerical simulations[1,2] of the electron beam–plasma instability assume the system to be spatially homogeneous and consider the evolution of the instability in time only. The infinite geometry theories are only capable of considering the development of instabilities caused by "single-shot" injection of the electron beam which limits the energy density of the excitation at the saturation level to be less than the energy density in the beam. In finite-length systems, fresh energy carried by the beam is continuously injected into the interaction region. The limitation of the saturation energy density will then be due to system nonlinearities rather than the geometry. Davis and Bers[3] have developed a charge-sheet model which takes the finite-length effect into account by assuming a boundary condition that all beam charge sheets are lost at the ends, whereas plasma charge sheets are reflected back into the system. This is equivalent to the assumption that the system is situated in an idealized "square-well" mirror magnetic field with a mirror ratio such that all beam-sheet velocities lie in the loss-cone region, and all plasma-sheet velocities lie outside of that region. They have observed many interesting phenomena such as meniscus formation, saturation of the instability in space, and the reduction of instability strength by a plasma density gradient in the direction of beam streaming.

In this investigation, the model of Davis and Bers is used to study saturation phenomena in electron beam–plasma interactions, both in space and time, and the phenomena of harmonic generation in frequency space. The effects of changes in system length and particle mass ratio on the ion beam–plasma instability are also investigated. The initial conditions for the numerical experiments are taken to correspond to a homogeneous plasma with a drifting beam ($V_{01}=100$). The beam is velocity modulated before it enters the interaction region with a 3% modulation depth at the electron plasma frequency. In the calculations, distance is normalized to the average plasma intersheet spacing and time to $1/\omega_{p0}$.

II. RESULTS OF ELECTRON BEAM–PLASMA INSTABILITY

The passage of an electron beam through a stationary plasma is capable of exciting plasma oscillations, and these oscillations will grow convectively at the expense of the dc energy of the electron beam. In all the cases considered the thermal conduction velocity (group velocity) of the plasma oscillations is approximately equal to $3v_{T2}^2/V_{01}$ and is much less than the dc velocity of the electron beam. Hence, the energy lost by the electron beam in the excitation of the plasma oscillations will accumulate in a small region at the plasma boundary. The fact that energy is fed into the plasma by the electron beam at a rate larger than that for which thermal conduction or other dissipative processes carry energy away will give rise to temporal growth.

Tsytovich[4] has advanced a general picture of the dynamic behavior of the electron beam–plasma instability in a semi-infinite system with a continuous injection of the electron beam. He predicted that the effective width of the intense-oscillation layer near the plasma boundary must decrease exponentially with time to a limiting value such that further growth of the oscillations is attended by a gradual motion of the saturation front away from the boundary and by the formation of a stationary electric-field distribution. To demonstrate Tsytovich's prediction, a numerical experiment is performed with the following parameters: interaction length ≈ 3 wavelengths ($2\pi V_{01}/\omega_{p0}$), $V_{T2}=8\times10^{-3}V_{01}$, and $\omega_{p1}^2=(1/80)\omega_{p0}^2$. The results for the inhomogeneous electric-field distribution at three

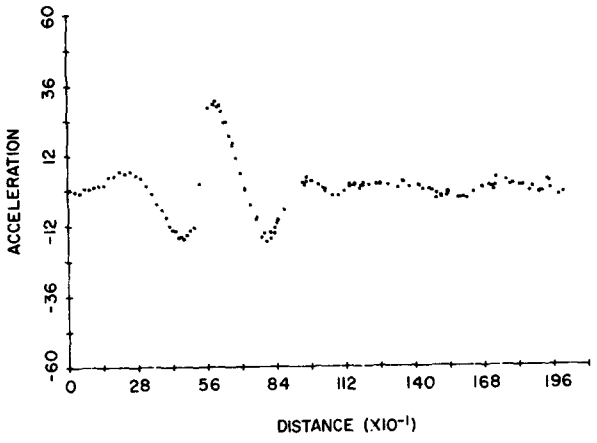

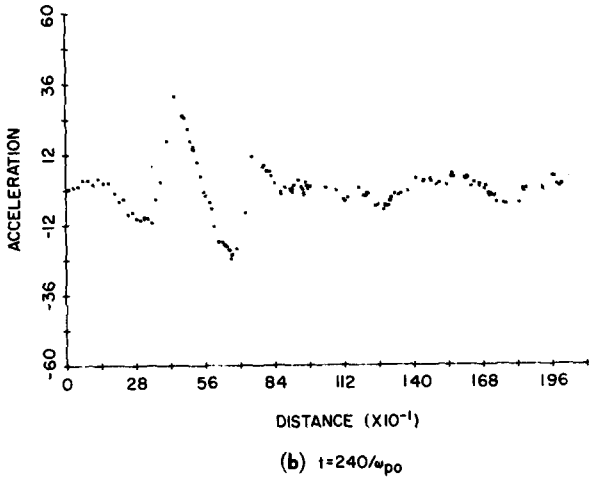

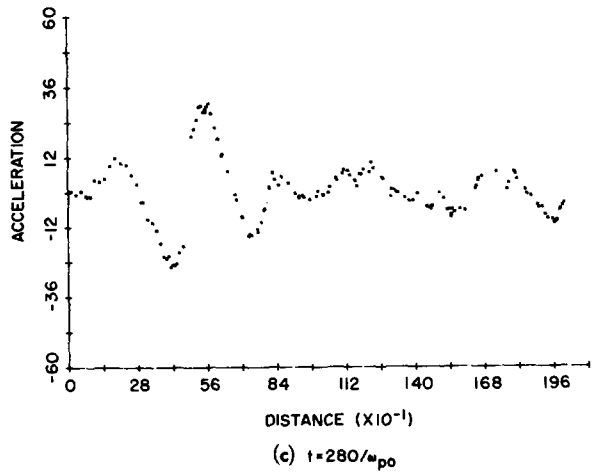

FIG. 1. Evolution of the acceleration for an electron beam–plasma system with $V_{T2}=8\times10^{-3}\ V_{01}$ and $\omega^2_{p1}=(1/80)\omega_{p0}^2$.

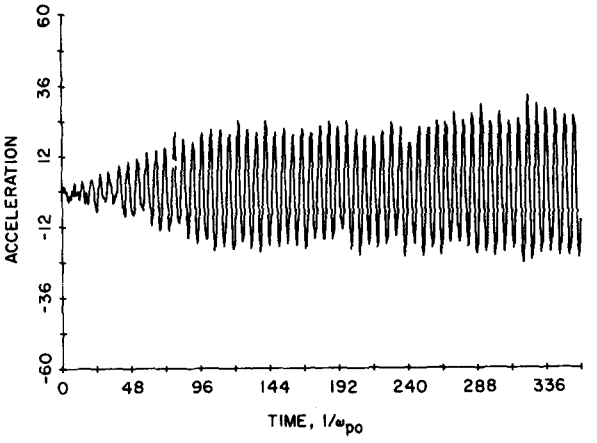

FIG. 2. Time evolution of the acceleration for an electron beam–plasma system with $V_{T2}=8\times10^{-2}\ V_{01}$ and $\omega_{p1}^2=(1/80)\omega_{p0}^2$ at $z=750$ $(0.01\ V_{01}/\omega_{p0})$.

different times are shown in Figs. 1–3; the field is normalized to $0.01V_{01}\omega_{p0}$. The electric field which is equivalent to the beam acceleration is observed to be highly inhomogeneous in the interaction region, and the amplitude of the high electric field increases and travels upstream as indicated in Figs. 1(a) and (b). This is equivalent to the high-field region narrowing with time. However, the increase in the energy of the excited large-amplitude oscillations in the narrow region gives rise to a rapid increase in the energy density gradient $d\bar{W}/dz$. Furthermore, the instability will heat the plasma which in turn will increase the group velocity (v_g) of the oscillations. The transfer of the oscillation energy from this narrow layer is determined by $v_g(d\bar{W}/dt)$.[4] After a sufficient time this mechanism must become decisive. In Fig. 1(c) it is seen that the

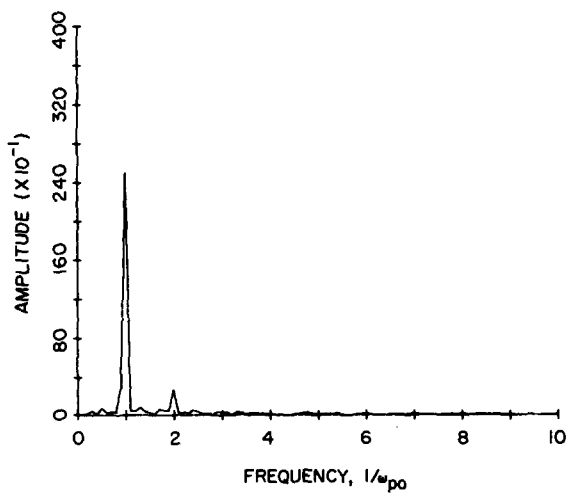

FIG. 3. Frequency spectrum at $z=750$ $(0.01\ V_{01}/\omega_{p0})$ for an electron beam–plasma system with $V_{T2}=8\times10^{-2}\ V_{01}$ and $\omega_{p1}^2=(1/80)\omega_{p0}^2$ at $t=320/\omega_{p0}$.

maximum of the beam acceleration (qE/m_e) at $t=280/\omega_{p0}$ occurs at a position farther downstream than that at $t=240/\omega_{p0}$ [Fig. 1(b)], and the amplitude of the beam acceleration is slightly reduced at this instant of time. Thus, the results of the numerical experiment are quantitatively in good agreement with the predictions of Tsytovich.

The results of the numerical experiment with $V_{T2}=8\times10^{-2}V_{01}$ reveal that the electric field at $z=750(0.01V_{01}/\omega_{p0})$ (Fig. 2) oscillates at the electron plasma frequency and saturates after sufficient time has elapsed. A crude explanation of the amplitude saturation phenomenon in the time domain can be obtained by describing the plasma as a nonlinear dielectric medium whose dielectric constant is dependent on the amplitude of the electric field. The equivalent dielectric constant for the plasma is[5]

$$\epsilon_p=\epsilon_0[1-(\omega_{p2}^2/\omega^2)\exp(-q^2\mid E\mid^2/8\omega^2m_ekT)]. \quad (1)$$

Whenever the plasma equivalent dielectric constant becomes negative, the beam electrons will attract one another rather than repel, such that any disturbance will grow. However, the nonlinear dielectric response implies that there exists a critical value of the electric-field amplitude $\mid E_c\mid$, such that the dielectric constant ϵ_p will be negative. Thus, the maximum value to which the electric field is allowed to grow can be determined. The oscillation frequency of the most unstable wave for an electron beam–plasma system occurs at[6]

$$\omega=\omega_{p0}[1-(\omega_{p1}/4\omega_{p2})^{2/3}]. \quad (2)$$

In this numerical experiment ω is equal to $0.91\omega_{p2}$. The substitution of this value into Eq. (1) gives $q\mid E_c\mid/m_e\simeq18(0.01V_{01}\omega_{p0})$ which is close to the simulation result $[q\mid E_c\mid/m_e\simeq24(0.01V_{01}\omega_{p0})]$.

In the nonlinear region the large-amplitude fundamental plasma oscillations excited by the electron beam will interact with themselves to generate harmonic components. Harmonic generation has been observed by Malmberg and Wharton[7] in their laboratory experiments on beam–plasma interactions. In our numerical experiments the results of the spectral analysis (Fig. 3) also exhibit harmonic generation. The amplitude of the harmonics is small in comparison with the fundamental because the plasma is nonresonant at these frequencies.

In the hydrodynamic approximation, the nonlinear differential equation for the electrostatic potential Φ in the unbounded cold beam–plasma system is[8]

$$\frac{d^2\Phi}{d\eta^2}=\frac{q}{\epsilon_0}\left[\frac{\eta_{10}(V_{01}-v_\varphi)}{[(2q/m_e)\Phi+(v_\varphi-V_{01})^2]^{1/2}}+\frac{\eta_{20}v_\varphi}{[(2q/m_e)\Phi+v_\varphi^2]^{1/2}}-\eta_0\right], \quad (3)$$

where $\eta=z-v_\varphi t$ and v_φ is the phase velocity of the wave. In this section the method of Bogoliubov and Mitropolsky[9] is used to solve Eq. (3). The nonlinearity arising from the plasma electrons will be neglected in this analysis since the density of the plasma is much larger than that of the electron beam in our numerical experiments. Next expand the right-hand side of Eq. (3) and retain all orders of Φ for the first term, but only the first order of Φ for the second term. Equation (3) is then simplified to

$$d^2\Phi/d\eta^2+\Omega_p^2\Phi=\epsilon f(\Phi), \quad (4)$$

where

$$f(\Phi)=(3q/2\epsilon_0)K^2\Phi^2-(5q/2\epsilon_0)K^3\Phi^3+\cdots, \quad (5)$$

$$\Omega_p^2=[\omega_{p1}^2/(v_\varphi-V_{01})^2]+(\omega_{p2}^2/v_\varphi^2), \quad (6)$$

$$K=q/m_e(v_\varphi-V_{01})^2, \quad (7)$$

and ϵ is a small positive parameter. The square-root expansion of the term $\{1+[2q\Phi/m_e(V_{01}-v_\varphi)^2]\}^{1/2}$ is permissible only in the case when the potential energy of the oscillations $q\Phi$ is less than the kinetic energy determined by the difference between the electron beam drift velocity and the wave phase velocity. Equation (4) is an equation for slightly nonlinear oscillations. The general solution of this equation may be written in the form

$$\Phi=a\cos\psi+\epsilon U_1(a,\psi)+\epsilon^2U_2(a,\psi)+\cdots, \quad (8)$$

where the quantities a and ψ are defined by the following differential equations:

$$da/d\eta=\epsilon A_1(a)+\epsilon^2A_2(a)+\cdots \quad (9)$$

and

$$d\psi/d\eta=\Omega_p+\epsilon B_1(a)+\epsilon^2B_2(a)+\cdots. \quad (10)$$

Substitute Eqs. (8)–(10) into Eq. (4). In the first approximation the coefficients of the first power of ϵ are equated on both sides of the resulting equation, and the following result is obtained:

$$\Omega_p^2\left(\frac{\partial^2U_1}{\partial\psi^2}+U_1\right)=f(a\cos\psi)+2\Omega_pA_1\sin\psi+2\Omega_paB_1\cos\psi. \quad (11)$$

To find proper expressions for the functions U_1, A_1, and B_1 the functions $f(a,\psi)$ and $U_1(a,\psi)$ are expanded into Fourier series as

$$f(a,\psi)=c_0(a)+\sum_{n=1}^{\infty}[c_n(a)\cos n\psi+d_n(a)\sin n\psi] \quad (12)$$

and

$$U_1(a,\psi)=e_0(a)+\sum_{n=1}^{\infty}[e_n(a)\cos n\psi+g_n(a)\sin n\psi]. \tag{13}$$

In terms of the Fourier components Eq. (11) becomes

$$\Omega_p^2 e_0(a)+\sum_{n=1}^{\infty}\Omega_p^2(1-n^2)[e_n(a)\cos n\psi+g_n(a)\sin n\psi]$$
$$=c_0(a)+[c_n(a)+2\Omega_p a B_1]\cos\psi+[d_1(a)+2\Omega_p A_1]\sin\psi$$
$$+\sum_{n=2}^{\infty}[c_n(a)\cos n\psi+d_n(a)\sin n\psi]. \tag{14}$$

Equating the coefficients of the same harmonics on both sides yields the following relations:

$$e_0(a)=c_0(a)/\Omega_p^2, \tag{15}$$

$$c_1(a)+2\Omega_p a B_1=0, \tag{16}$$

$$d_1(a)+2\Omega_p A_1=0, \tag{17}$$

$$e_n(a)=c_n(a)/\Omega_p^2(1-n^2), \tag{18}$$

and

$$g_n(a)=d_n(a)/\Omega_p^2(1-n^2), \tag{19}$$

where $n=2, 3, \cdots$. The terms $e_1(a)$ and $g_1(a)$ are chosen to be zero for nonsecular solutions[9] and, thus,

$$U_1(a,\psi)=\frac{c_0(a)}{\Omega_p^2}+\frac{1}{\Omega_p^2}\sum_{n=2}^{\infty}\frac{c_n(a)\cos n\psi+d_n(a)\sin n\psi}{1-n^2}. \tag{20}$$

Hence, explicit expressions have been obtained for $A_1(a)$, $B_1(a)$, and $U_1(a,\psi)$ in terms of the Fourier expansion of $f(a\cos\psi)$.

For simplicity only the first two terms of Eq. (5) are retained and, after using the multiple angle formulas for cosine functions, it can be written as

$$f(\Phi)=\frac{3qK^2a^2}{4\epsilon_0}-\frac{15qK^3a^3}{8\epsilon_0}\cos\psi$$
$$+\frac{3qK^2a^2}{4\epsilon_0}\cos2\psi-\frac{5qK^3a^3}{8\epsilon_0}\cos3\psi. \tag{21}$$

Equation (21) is in the form of a Fourier series in which only cosine components up to third harmonic are presented. From Eq. (17) the following can be seen:

$$A_1=-d_1(a)/2\pi\Omega_p=0.$$

It follows from Eq. (9) that the amplitude a is independent of η. This result is not surprising since in deriving Eq. (3) it is assumed that all oscillating quantities are functions only of $(z-v_\varphi t)$ which implies that only nonlinear stationary waves exist. B_1 can be found from Eq. (16),

$$B_1=-c_1(a)/2a\Omega_p=15qa^2K^3/16\epsilon_0\Omega_p. \tag{22}$$

Hence, ψ can be determined from Eq. (10),

$$\psi=[\Omega_p+\epsilon(15qa^2K^3/16\epsilon_0\Omega_p)]\eta+\theta, \tag{23}$$

where θ is the initial phase angle. Substituting the expressions for $c_0(a)$, $c_2(a)$, and $c_3(a)$ from Eq. (17) into Eq. (16) gives

$$U_1(a,\psi)=\frac{3qK^2a^2}{4\epsilon_0\Omega_p^2}-\frac{qK^2a^2}{4\epsilon_0\Omega_p^2}\cos2\psi+\frac{5qK^3a^3}{64\epsilon_0\Omega_p^2}\cos3\psi. \tag{24}$$

Thus, the following solution is obtained in the first approximation:

$$\Phi=a\cos\psi+\epsilon\left(\frac{3qK^2a^2}{4\epsilon_0\Omega_p^2}-\frac{qK^2a^2}{4\epsilon_0\Omega_p^2}\cos2\psi+\frac{5qK^3a^3}{64\epsilon_0\Omega_p^2}\cos3\psi\right). \tag{25}$$

It is evident from Eq. (21) that second and third harmonics have been generated. The fundamental frequency is determined by Eq. (23), and it depends on the amplitude. The amplitudes of the second and third harmonics are proportional to the square and cube of the amplitude of the fundamental, respectively. This result is in agreement with the experimental results of Malmberg and Wharton.[7] If all the terms in Eq. (5) are retained, all the harmonic components are expected to be generated.

III. RESULTS OF ION BEAM-PLASMA INSTABILITY SIMULATION

The energy transfer from the electron beam to the plasma is decreased by the deceleration and thermal spread of the electron beam caused by the reaction of the excited plasma oscillations on the electron beam. On the basis of this consideration, as well as others, the ion beam–plasma interaction is investigated in order to take advantage of the heavier ion mass, which is expected to yield a larger energy source, a low rate of decrease in the mean ion-beam speed, and a slower thermal spreading of the ion-beam velocity in comparison with the interaction between an electron beam and a similar plasma. The beam–plasma instability can reach very large amplitudes which suggests that the decaying process[4] of the excited oscillations might be substantial. This phenomenon is allowed to develop in the two-component sheet model used in the simulation of the ion beam–plasma instability. The parameters used in these numerical experiments are basically

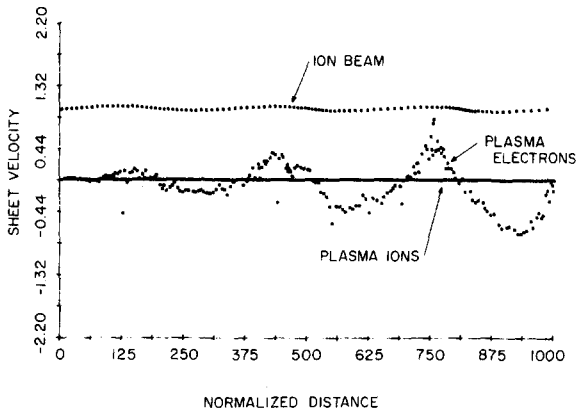

FIG. 4. Phase space plots for an ion beam–plasma interaction at $t=120/\omega_{p0}$ with $m_i/m_e=1000$, system length $L\approx 3$ wavelengths.

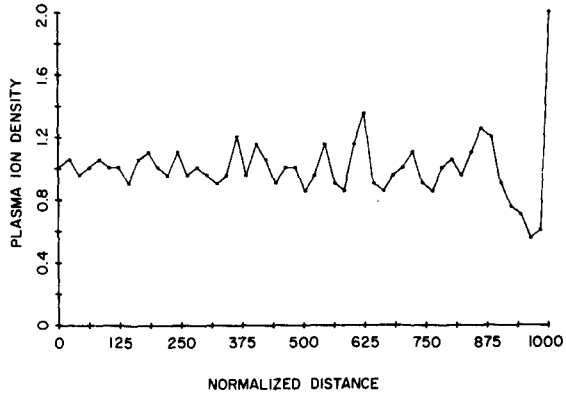

FIG. 6. Plasma ion density distribution for an ion beam–plasma interaction at $t=200/\omega_{p0}$ with $m_i/m_e=1000$, system length $L\approx 3$ wavelengths.

the same as in the previous experiments except that an ion beam replaces the electron beam as the energy source, and the beam drifting velocity is reduced to half that of the electron-beam velocity and ω_{p1}^2 is equal to 1/40 of ω_{p0}^2. Initially, the plasma ion thermal velocity is zero and that of the electron, $8\times 10^{-3}V_{01}$.

In the first experiment the ions are 1000 times heavier than the electrons, and the interaction length is taken to be approximately three wavelengths. The excitation of electron plasma oscillations is observed in the numerical experiments. In response to the resulting electric field the ion-beam velocity is only slightly perturbed due to the heavy mass of the ions, and it remains laminar throughout the process, whereas the plasma electrons because of their great mobility rapidly gain kinetic energy (Fig. 4) and exhibit a vortex formation with respect to the ion beam in phase space. In the initial stages the electric field behaves like that observed in the electron beam–plasma interaction, i.e., the maximum of the electric field increases in amplitude and travels upstream. However, at a later time, the beam–plasma instability is observed to decay. This phenomenon is displayed clearly in the time evolution of the electric-field energy (Fig. 5) in which the energy initially grows with an exponential growth rate of approximately $0.041\omega_{p0}$ which is approximately one half of the value predicted by the linear theory ($0.0866\omega_{p0}$). At $t=120/\omega_{p0}$ the energy begins to decay. This decay phenomenon is also observed by Kruer and Dawson[10] in their investigation of the damping of a large-amplitude electric field in a two-component plasma. The numerical results indicate that the plasma ion density distribution (Fig. 6) acquires a large spatial fluctuation at $t=200/\omega_{p0}$ when the electric-field energy decays to a small value. This may be interpreted as an electric-field energy dissipation occurring when the intensity of the ion beam–plasma instability exceeds some threshold value in association with the excita-

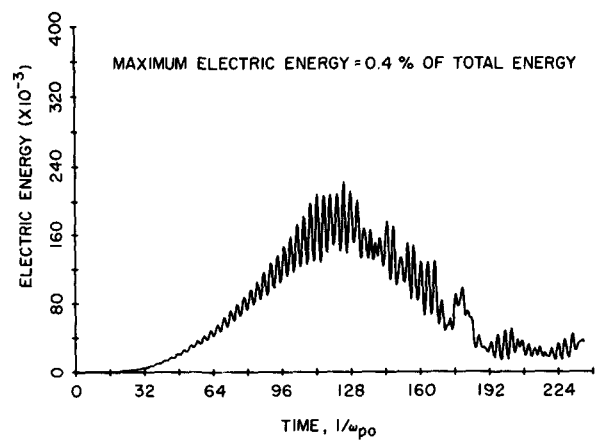

FIG. 5. Electric energy vs time for an ion beam–plasma interaction with $m_i/m_e=1000$, system length $L\approx 3$ wavelengths.

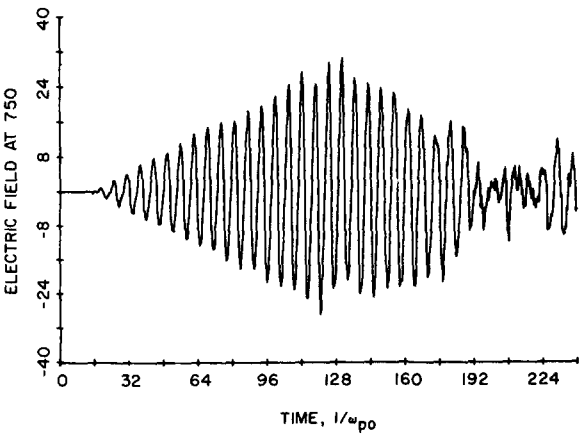

FIG. 7. Electric field vs time for an ion beam–plasma interaction at $z=750$ ($0.02\ V_{01}/\omega_{p0}$) with $m_i/m_e=1000$, system length $L\approx 3$ wavelengths.

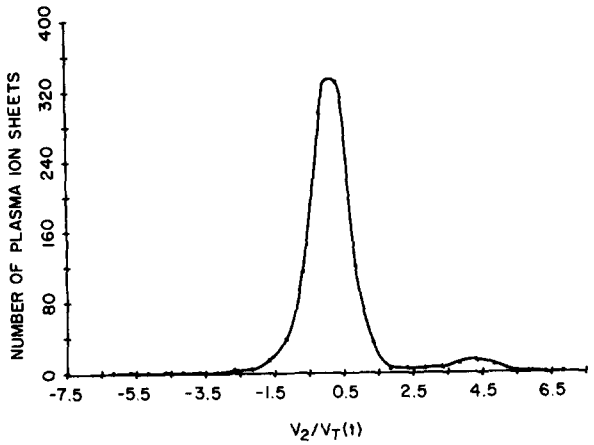

FIG. 8. Plasma ion velocity distribution for an ion–beam interaction at $t=160/\omega_{p0}$ with $m_i/m_e=1000$, system length $L\approx 3$ wavelengths. [$V_T(t)$ = instantaneous values of the plasma ion thermal velocity.]

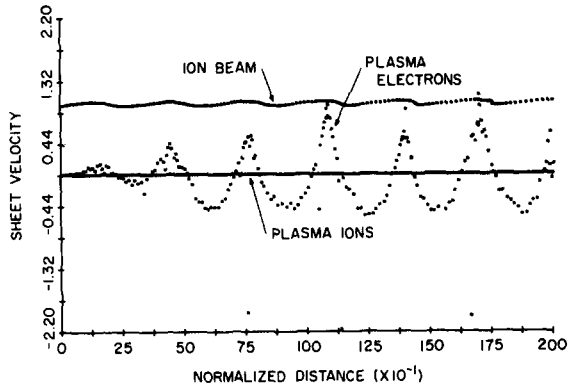

FIG. 10. Phase space plots for an ion beam–plasma interaction at $t=120/\omega_{p0}$ with $m_i/m_e=1000$, system length $L\approx 6$ wavelengths.

tion of large-amplitude ion-density fluctuations as suggested by Kruer and Dawson.

There are, of course, other possible mechanisms responsible for the decaying process. Tsytovich[4] indicates that large-amplitude plasma oscillations could possibly decay into ion-acoustic oscillations. Figure 7 shows the time evolution of the electric field at position $z=750(0.02V_{01}/\omega_{p0})$. The electric field oscillates at the electron-plasma frequency and is amplitude modulated at the ion-acoustic frequency. During the initial stages, plasma electrons are trapped by the excited electron plasma oscillations and the oscillatory energy contributes primarily to the plasma kinetic energy. At later times the oscillatory energy is converted into random energy, and then a characteristic plasma electron temperature can be defined. The heating of the plasma electrons is much more rapid than the heating of the plasma ions in this experiment. Figure 8 gives the plasma ion velocity distribution function at $t=160/\omega_{p0}$ which indicates the development of a small high-temperature tail on the positive velocity side, that is, on the side of the beam-drift velocity. The velocity at which the small high-temperature tail peaks is of the order of the ion-acoustic velocity, which suggests that at this time the ion-acoustic wave has grown to an amplitude large enough to trap a significant number of plasma-ion sheets. Another case in which the particle mass ratio is taken to be 100 is also studied, and much more ion heating and less electron heating is observed. The excited plasma oscillations (Fig. 9) begin to decay at an earlier time ($t\approx 84/\omega_{p0}$) than in the previous case, and the modulation period is reduced to the appropriate ion-acoustic period. These show that the nonlinear heating and decaying phenomena do depend on the mass ratio.

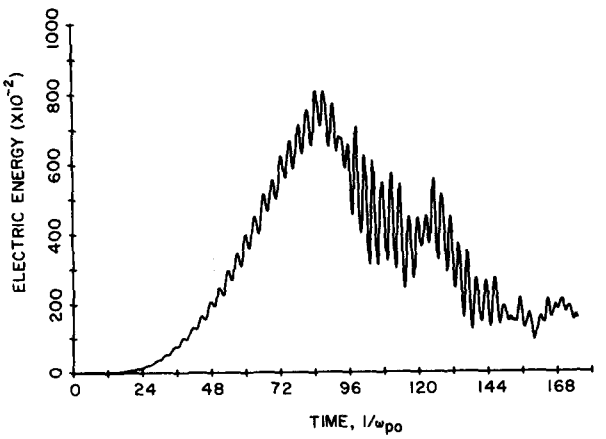

FIG. 9. Electric-field energy vs time for ion beam-plasma interaction with $m_i/m_e=100$, system length $L\approx 3$ wavelengths.

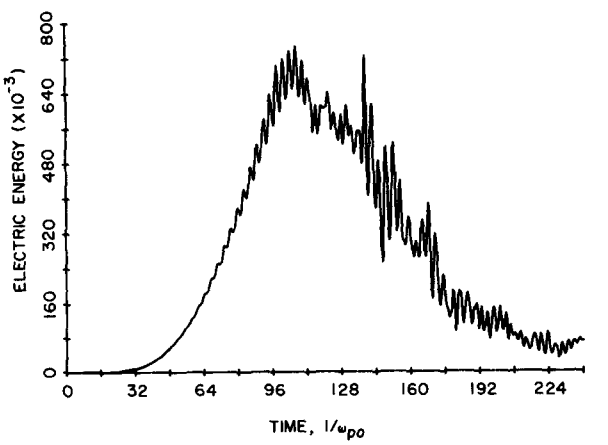

FIG. 11. Electric energy vs time for an ion beam–plasma interaction with $m_i/m_e=1000$, system length $L\approx 6$ wavelengths.

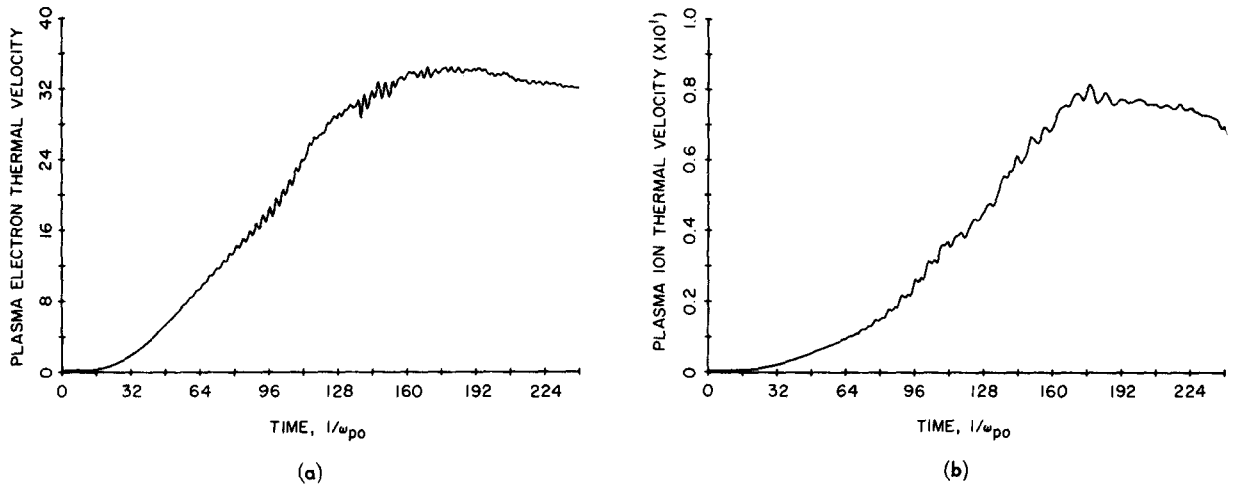

FIG. 12. Plasma thermal velocities vs time for an ion beam–plasma interaction with $m_i/m_e = 1000$, system length $L \approx 6$ wavelengths. (a) Plasma electron thermal velocity; (b) plasma ion thermal velocity.

Another case with a mass ratio of 1000 and system length of approximately six wavelengths (Fig. 10) is also investigated. Doubling the interaction length approximately triples the maximum attainable electric-field energy of the system and, thus, results in the decaying process occurring at an earlier time ($t \approx 100/\omega_{p0}$) (Fig. 11) than in the first experiment. The maximum plasma electron [Fig. 12(a)] and ion [Fig. 12(b)] thermal velocities have reached 75% and 0.6% of beam drifting speed, respectively.

IV. SUMMARY

The results of the computer simulation of an electron beam–plasma instability in a finite-length one-dimensional system indicate that the electric field is highly inhomogeneous in the interaction region. The width of the high-field region decreases with time to a limiting value then increases with a reduction in the electric-field amplitude to form a stationary distribution. The harmonic generation in frequency space is also observed.

In the ion beam–plasma interactions, the instability decays when the intensity of the instability exceeds some threshold level which depends on the particle mass ratio and interaction length. This decay phenomenon is associated with the excitation of large-amplitude ion-density fluctuations and ion-acoustic oscillations. The plasma achieves higher heating in comparison with the interaction between an electron beam and a plasma. The heating also depends on the particle mass ratio.

ACKNOWLEDGMENT

The work was made possible through the sponsorship of the National Science Foundation under Research Grant No. GK-15689 and is gratefully acknowledged.

[1] R. L. Morse and C. W. Nielson, Phys. Fluids **12**, 2418 (1969).
[2] R. L. Morse and C. W. Nielson, Phys. Rev. Letters **23**, 1087 (1969).
[3] J. A. Davis and A. Bers, in *Turbulence of Fluids and Plasma* (Polytechnic Institute of Brooklyn Press, Brooklyn, New York, 1969), p. 87.
[4] V. N. Tsytovich, *Nonlinear Effects in Plasma* (Plenum, New York, 1970), Chap. 6.
[5] A. V. Gurevich and L. P. Pitaevskii, Zh. Eksp. Teor. Fiz. **45**, 1243 (1963) [Sov. Phys. JETP **18**, 855 (1964)].
[6] W. E. Drummond, J. H. Malmberg, T. M. O'Neil, and J. R. Thompson, Phys. Fluids **13**, 2422 (1970).
[7] J. H. Malmberg and C. B. Wharton, Phys. Fluids **12**, 2600 (1969).
[8] H. K. Sen, Phys. Rev. **27**, 849 (1955).
[9] N. N. Bogoliubov and Y. A. Mitropolsky, *Asymptotic Methods in the Theory of Nonlinear Oscillations* (Hindustan, Delhi, 1961), Chap. 1.
[10] W. L. Kruer and J. Dawson, Phys. Rev. Letters **25**, 1174 (1970).